Supplement of Saf. Nucl. Waste Disposal, 1, 179–180, 2021
https://doi.org/10.5194/sand-1-179-2021-supplement

Supplement of

Hydro-mechanical effects of seismic events in crystalline rock barriers

Dominik Kern et al.

Correspondence to: Dominik Kern (dominik.kern1@ifgt.tu-freiberg.de)

TECHNISCHE UNIVERSITÄT BERGAKADEMIE FREIBERG
The University of Resources. Since 1765.

Federal Office for the Safety of Nuclear Waste Management

Hydro-mechanical effects of seismic events in crystalline rock barrier

Dominik Kern[1], Fabien Magri[2,3], Victor I. Malkovsky[4], Thomas Nagel[1]

MOTIVATION

Under ideal conditions, owing to its extremely low matrix permeability, crystalline rock can constitute a suitable hydro-geological barrier. Mechanically, its high strength and stiffness provide advantages when constructing a repository and for long-term stability.
However, crystalline rock usually occurs in a fractured form which can drastically alter hydro-mechanical (HM) barrier functions due to increased permeability and decreased strength. Seismic events have the potential to alter these HM properties by activating faults, increasing their transmissibility, creating new fractures or altering network connectivity [1]. Therefore it is of high importance to build computational models allowing to assess the HM effects of seismic events in a Deep Geologic Repository (DGR) in crystalline rock, as illustrated in Figure 1.
The Noordbergum effect and the Mandel-Cryer effect are well-known examples of HM coupling [2] and we expect similar patterns in the model of an exemplary storage site for nuclear waste. Particularly, we focus on the consequences of the time-dependent pressure and stress fluctuations after a change of the stresses in the ground. Such stress changes and stress redistributions may occure after earthquakes [3]–[5] and affect even distant areas.
Here, we present a coupled HM simulation, using OpenGeoSys [6], of a large-scale, three-dimensional finite-element model of the Yeniseysky Site (YS) in Russia to assess the consequences of seismically induced stress-field changes on the local stress field.

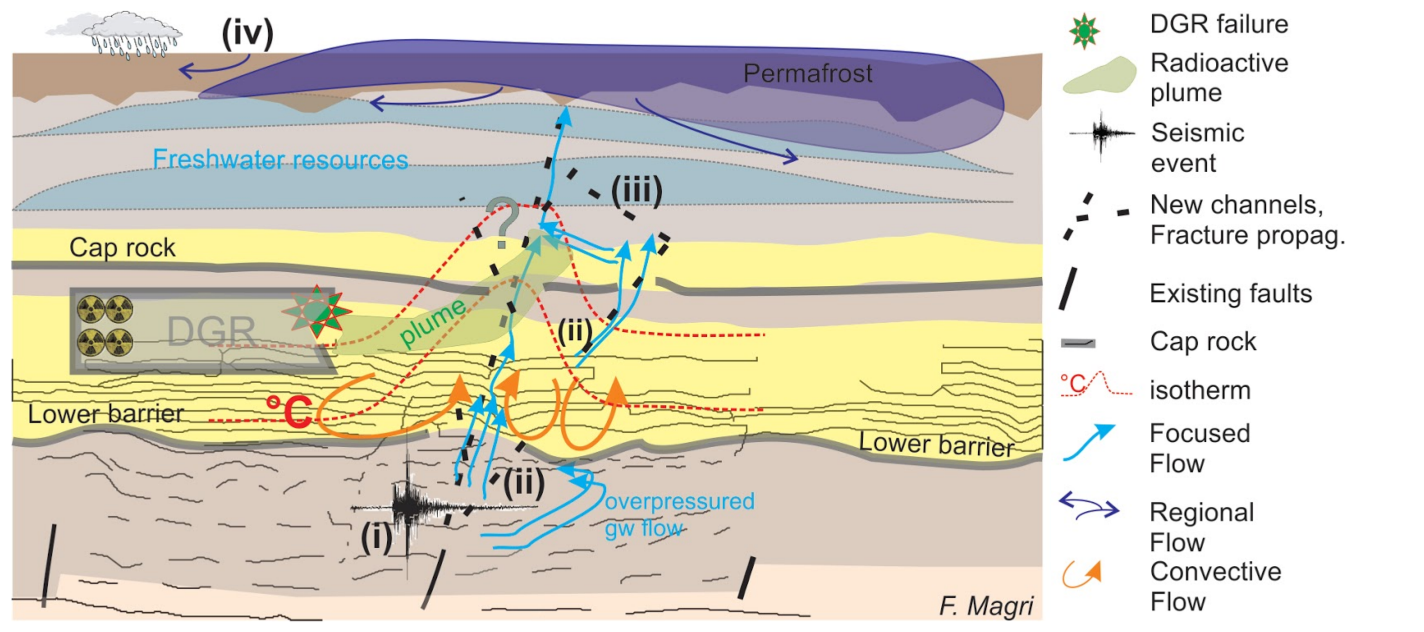

Fig. 1: Most relevant events for the integrity of a DGR in crystalline rock (i) Cap-rock failure due to seismic events, (ii) focused flow escapes from the aquifer, (iii) flow-induced fractures propagate generating a heterogeneous porosity-permeability field, (iv) Changing climate/permafrost impacts [7].

MODEL

As an example, we consider YS [8] for high-level waste in crystalline rock which is located close to a potentially seismically active area.

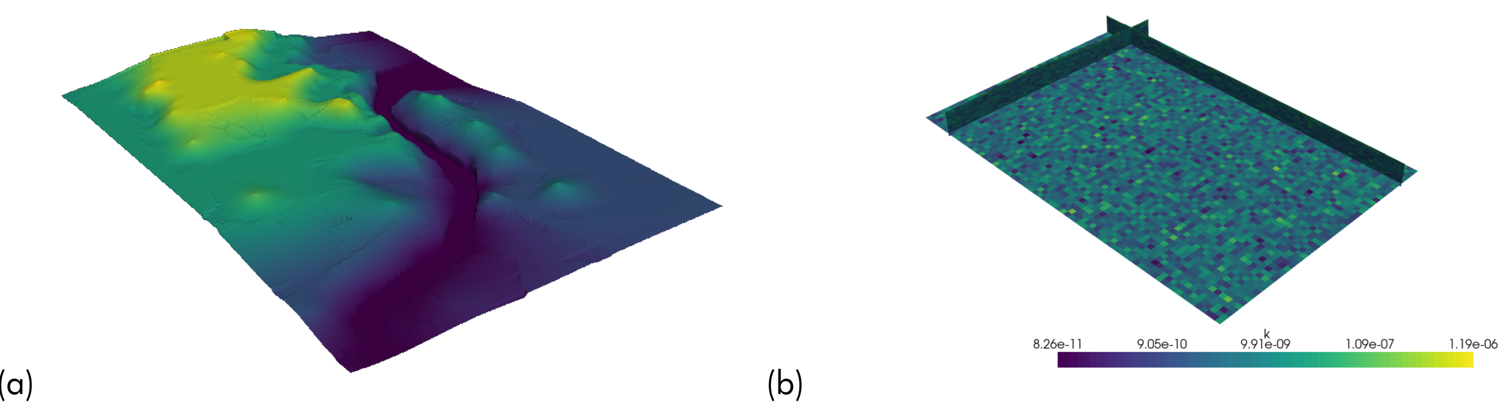

Fig. 2: Earth surface at YS (a) and hydraulic conductivity ($\mathrm{m\,s^{-1}}$) distribution [8] shown in three orthogonal slices (b)

Deep Geological Repository

The DGR is located in a depth of $z = -400$ m to -500 m under the earth surface shown in Figure 2(a). Vitrified high-level waste and long-lived intermediate-level waste are to be emplaced on two levels covering an area of 317 m×745 m.

Geology and Hydrology

The site is located in Southern Siberia and lies on the southwestern edge of the Siberian shield. It consists of Archaean and Proterozoic gneiss complexes and is covered by Quaternary rocks.
Hydrologically this region belongs to the catchment area of Yenisey river. The site itself is located on the watersheds between Yenisey and another river.
The site is in a compression regime, the horizontal stresses in average $\sigma_{\mathrm{h}}(z = -500\,\mathrm{m}) = 13.5$ MPa are higher than they would be due to gravitation only [8]. In a distance of 100 km to 1000 km earthquakes occured and seismic activity has been recorded in the last 200 years [9].

Physical Properties

The physical parameters, listed in Table 1, are estimated from borehole logs, geophysical measurements and laboratory experiments. Figure 2(b) shows the estimated distribution of hydraulic conductivity.

Tab. 1: Physical properties [9]

name	symbol	value/range
fluid density	ρ_{f}	$1 \times 10^3\,\mathrm{kg\,m^{-3}}$
fluid viscosity	μ	$1 \times 10^{-3}\,\mathrm{Pa\,s}$
solid density	ρ_{s}	$2.7 \times 10^3\,\mathrm{kg\,m^{-3}}$ to $3.5 \times 10^3\,\mathrm{kg\,m^{-3}}$
Young's modulus (bulk, drained)	E	5.63×10^{10} Pa to 7.87×10^{10} Pa
Poisson's ratio (bulk, drained)	ν	0.21 to 0.28
porosity	ϕ	0.15 % to 0.5 %
Biot coefficient	α	1.0
hydraulic conductivity	k	$8 \times 10^{11}\,\mathrm{m\,s^{-1}}$ to $1 \times 10^{6}\,\mathrm{m\,s^{-1}}$

Field Equations

We use the simplified equation set ($\mathbf{u}$-p form) for quasistatic, fully saturated, poroelastic media [10]

$$\alpha\frac{\partial \varepsilon}{\partial t} + S\frac{\partial p}{\partial t} + \nabla\cdot\mathbf{q} = 0 \quad \text{with} \quad \varepsilon = \nabla\cdot\mathbf{u} \quad \text{and} \quad \mathbf{q} = -\frac{k}{\gamma_{\mathrm{w}}}(\nabla p - \rho_{\mathrm{f}}\mathbf{g}), \tag{1}$$

$$\nabla\cdot\boldsymbol{\sigma} + \rho\mathbf{b} = \mathbf{0} \quad \text{with} \quad \boldsymbol{\sigma} = \mathbb{C} : \boldsymbol{\varepsilon} - \alpha p\mathbf{1} \quad \text{and} \quad \boldsymbol{\varepsilon} = \nabla_{\mathrm{s}}\otimes\mathbf{u}. \tag{2}$$

Since the hydraulic conductivity distribution [11] is provided in higher resolution than the remaining parameters, we consider it as guiding for the others. In a first approximation we use a linear interpolation within their ranges. We assume that the higher the hydraulic conductivity the lower the elastic stiffness ($k\uparrow E\downarrow$) and the higher the porosity ($k\uparrow \phi\uparrow$).

Boundary Conditions

As Figure 3 shows, we impose atmospheric pressure on top and impermable boundaries elsewhere (watersheds, impermable bedrock). The normal stresses applied at the lateral boundaries are linearly increasing with depth. The bottom is fixed in vertical direction, as is one side for each direction in space. Starting from an equilibrated initial state we simulate two load cases, similarly to observations elsewhere [5]: *stress increase* and *stress rotation*. In the former case, the stresses increases uniformly (factor $6/5$), whereas in the latter case the stress field rotates at constant mean stress (factor $6/5$ in x-direction and $4/5$ in y-direction). In both cases the stress change occurs in the time $t = 20 \times 10^5\,\mathrm{s} \ldots 25 \times 10^5\,\mathrm{s}$.

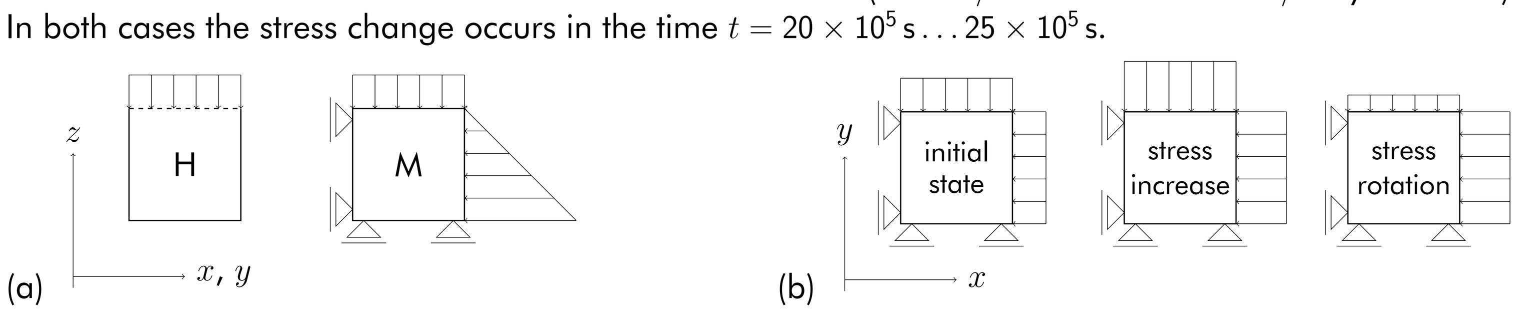

Fig. 3: Hydraulical and mechanical boundary conditions remain qualitatively the same in front and side view (a), whereas in top view there appears the change from the initial state to one of the final states (b)

Discretization

We use the open-source multi-physics finite-element software OpenGeoSys [6] to solve the coupled hydro-mechanical problem. The spatial discretization is done by hexahedral Taylor-Hood elements, as shown in Figure 4(a). The material parameters are assigned blockwise. As time discretization we have chosen an Euler-backward scheme. The discretization parameters are listed in Table 2 and the mesh is shown in Figure 4(b).

Tab. 2: Discretization parameters

domain	blocks	element size	time step
12.5 km×18.2 km×1.5 km	250 m×250 m×50 m	50 m×50 m×50 m	$5 \times 10^5\,\mathrm{s} \approx 5.8\,\mathrm{d}$

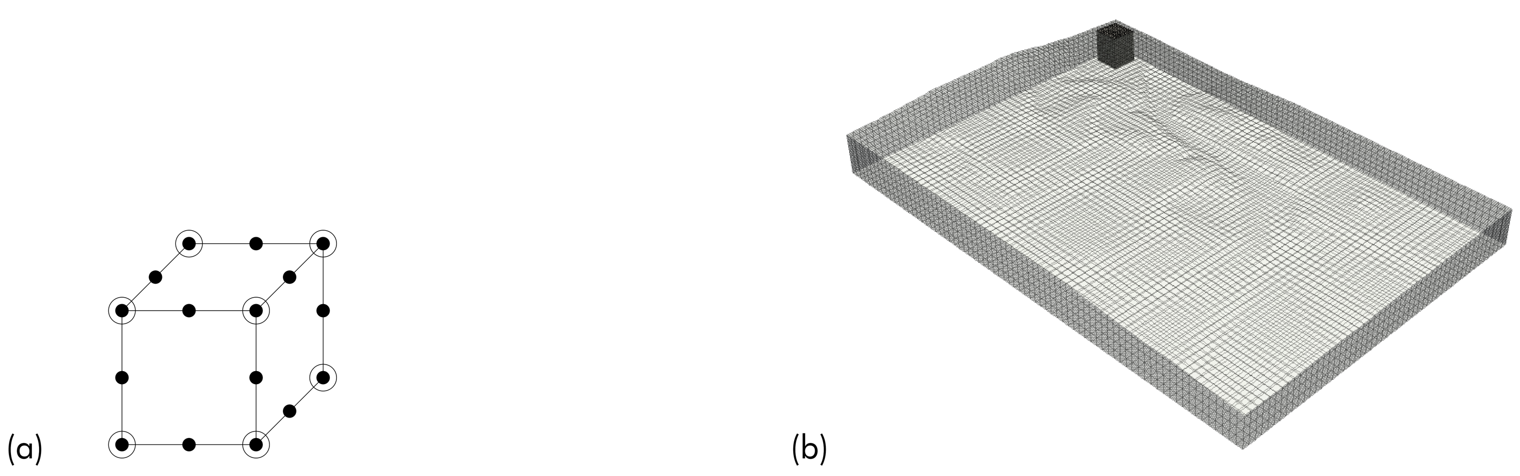

Fig. 4: Hexahedral Taylor-Hood Element with 8 nodes for pressure and 20 nodes for displacements (a), discretized domain and used mesh (b).

RESULTS AND OUTLOOK

For the first load case *stress increase* we observe in Figure 5 that the effective deviatoric stresses, collected in the von-Mises stress q, increase as the total stresses do. Whereas the fluid (pressure p) carries the added total mean stress first and shifts it slowly to the solid (effective mean stress p').

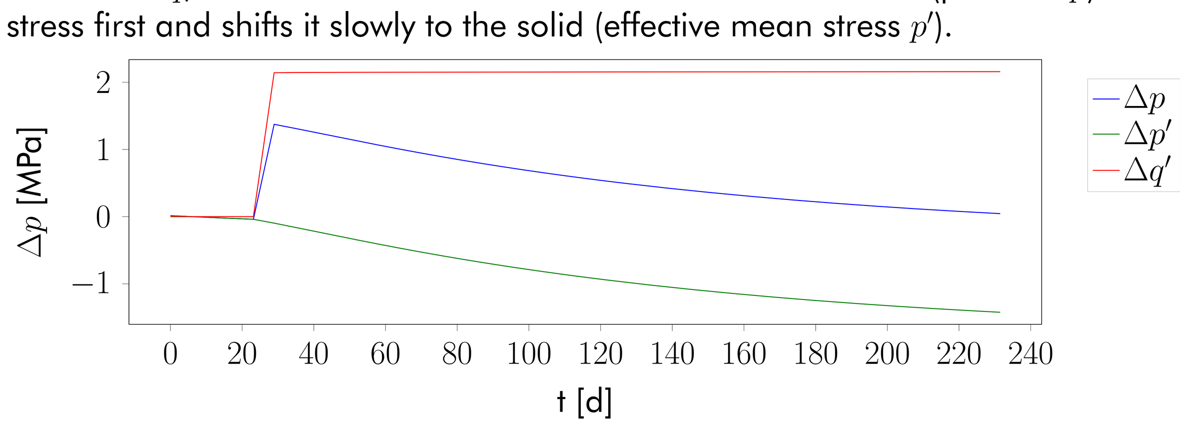

Fig. 5: Changes of fluid pressure, effective mean stress and effective deviatoric stress (von Mises) in the center of the model for load case *stress increase*.

A rotation of the horizontal stress, as in the second load case, does not change the total mean stress and so it changes neither the fluid pressure nor the effective mean stress. Still, there is a change in the deviatoric stresses.

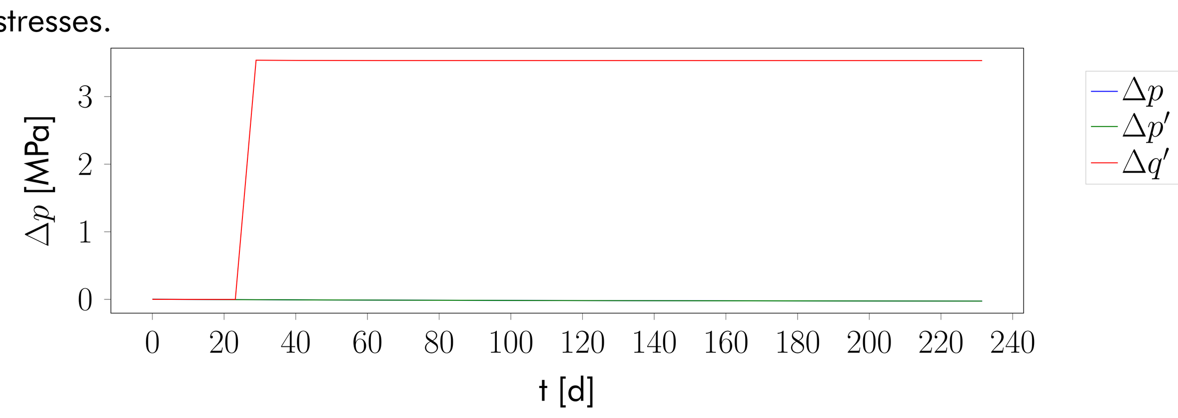

Fig. 6: Same as Figure 5, but for load case *stress rotation*.

As future work, we are going to refine the scenarios and to analyze: fault-slip potentials, parameter dependencies and fully dynamic models.

[1] V. De Rubeis, Z. Czechowski, and R. Teisseyre, *Synchronization and Triggering: from Fracture to Earthquake Processes*. Springer, 2010.
[2] C. E. Neuzil, "Hydromechanical coupling in geologic processes", *Hydrogeology Journal*, vol. 11, no. 1, pp. 41–83, 2003, ISSN: 14312174. DOI: 10.1007/s10040-002-0230-8.
[3] C. Wang, C. Song, Q. Guo, J. Mao, and Y. Zhang, "New insights into stress changes before and after the Wenchuan Earthquake using hydraulic fracturing measurements", *Engineering Geology*, vol. 194, pp. 98–113, 2015, ISSN: 00137952. DOI: 10.1016/j.enggeo.2015.05.016. [Online]. Available: http://dx.doi.org/10.1016/j.enggeo.2015.05.016.
[4] D. Marsan, "The role of small earthquakes in redistributing crustal elastic stress", *Geophysical Journal International*, vol. 163, no. 1, pp. 141–151, 2005, ISSN: 0956540X. DOI: 10.1111/j.1365-246X.2005.02700.x.
[5] "Temporal Stress Changes Caused by Earthquakes: A Review", *Journal of Geophysical Research: Solid Earth*, vol. 123, no. 2, pp. 1350–1365, 2018, ISSN: 21699356. DOI: 10.1002/2017JB014617.
[6] O. Kolditz, U.-J. Goerke, H. Shao, and W. Wang, *Thermo-hydro-mechanical-chemical processes in porous media: benchmarks and examples*. Springer Science & Business Media, 2012, vol. 86.
[7] F. Magri, T. Nagel, A. Liebscher, and V. Malkovsky, "Impacts of changing conditions on far-field radionuclide evolution: Background and goals of a newly funded dfg-rfbr project.", in *EGU General Assembly Conference Abstracts*, 2020, p. 17 712.
[8] B. Kochkin, V. Malkovsky, and S. Yudinzev, "Scientific basis for assessing the safety of geological isolation of long-lived radioactive waste (in russian)", *IGEM RAN*, 2017.
[9] M. Jobmann, "Site-specific evaluation of safety issues for high-level waste disposal in crystalline rocks. final report", DBE Technology GmbH, Tech. Rep., 2016.
[10] O. C. Zienkiewicz, A. Chan, M. Pastor, B. Schrefler, and T. Shiomi, *Computational geomechanics*. Citeseer, 1999, vol. 613.
[11] A. Ozerskiy, "Hydrogeology of the archean crystalline rock massif in the southern part of the yenisseyskiy ridge (siberian craton)", *On the surface*, vol. 3, p. 10, 2017.

Acknowledgment
Funded by
DFG Deutsche Forschungsgemeinschaft
German Research Foundation
RFBR RUSSIAN FOUNDATION FOR BASIC RESEARCH

[1]Institute for Geotechnics
TU Bergakademie Freiberg
Freiberg, Germany

[2]Division Task-related Research
Federal Office for the Safety of Nuclear Waste Management
Berlin, Germany

[3]Institute of Geological Sciences
Freie Universität Berlin
Berlin, Germany

[4]Institute of Geology of Ore Deposits and Petrography and Mineralogy and Geochemistry
Russian Academy of Sciences
Moscow, Russia

Corresponding author: Dominik Kern (dominik.kern1@ifgt.tu-freiberg.de)